J Mol Model (2012) 18:1255–1262
DOI 10.1007/s00894-011-1155-8

ORIGINAL PAPER

Density functional theory analysis of carbonyl sulfide hydrolysis: effect of solvation and nucleophile variation

Ri-Guang Zhang · Li-Xia Ling · Bao-Jun Wang

Received: 8 November 2010 / Accepted: 15 June 2011 / Published online: 7 July 2011

Abstract The detailed mechanisms of the hydrolysis of carbonyl sulfide (OCS) by nucleophilic water and hydroxide ion in both the gas phase and bulk water solvent have been investigated using density functional theory. Various reaction channels on the potential surface have been identified. The thermodynamic results demonstrate that the hydrolysis of OCS by nucleophilic water and hydroxide ion should proceed more favorably at low temperature. The hydrolysis of OCS by the hydroxide ion is the main reaction channel from thermodynamic and kinetic perspectives, and the bulk solvent can influence the rate-determining step in this channel. However, the solvent barely modifies the activation energy of the rate-determining step. For the hydrolysis of OCS by nucleophilic water, the solvent does not modify the rate-determining step, and the corresponding activation energy of the rate-determining step barely changes. This bulk solvent effect suggests that most of the contribution of the solvent is accounted for by considering one water molecule and a hydroxide ion.

Keywords Carbonyl sulfide · Hydrolysis · OH^- · H_2O · Thermodynamics · Kinetics · Density functional theory

Introduction

Over the last two decades, it has become increasingly apparent that emissions of sulfur compounds into the atmosphere have been unacceptably high. Recently, increasingly stringent emission standards have been introduced around the world in order to reduce emissions of sulfur-containing compounds into the atmosphere [1]. Carbonyl sulfide (OCS), which is the by-product of many chemical processes involved in the conversion of fossil fuels, is thought to be one of the major components of organic sulfur compounds [2]. The hydrolysis of OCS is considered a promising process due to its mild reaction conditions and high conversion efficiency [3]. There have been numerous experimental studies of the hydrolysis mechanism of OCS [4–12]. The distinct channels for the hydrolysis of OCS by nucleophilic water and hydroxide ion can be represented stoichiometrically using the reactions below:

$$OCS + H_2O = H_2S + CO_2 \quad (1)$$

$$OCS + OH^- = SH^- + CO_2. \quad (2)$$

However, to gain a detailed understanding of the OCS hydrolysis mechanism, experimental data is not always sufficient; theoretical calculations can be helpful in order to clarify some essential questions. Quantum chemical methods have become useful tools for determining reaction mechanisms. With recent developments in theoretical methodology, density functional theory (DFT) is now capable of providing qualitative and quantitative insights into reaction mechanisms [13, 14]. While there have already been some theoretical studies of the hydrolysis mechanism of OCS, they have all modeled the reaction at metal oxide surfaces [15, 16]. To the best of our knowledge, few theoretical studies of the hydrolysis of OCS in pure water have been reported; such studies would be helpful for

R.-G. Zhang · L.-X. Ling · B.-J. Wang (✉)
Key Laboratory of Coal Science and Technology of Ministry of Education and Shanxi Province,
Taiyuan University of Technology,
Taiyuan 030024, China
e-mail: wangbaojun@tyut.edu.cn

deeply probing the mechanism of hydrolysis from the viewpoint of quantum chemistry. Deng et al. [3] have investigated the mechanism for hydrolysis reaction (1) in the presence of up to five water molecules, but, as we shall see, this reaction is somewhat different from those presented in this study. Meanwhile, reaction (2) was not mentioned in the studies of Deng et al. In fact, reaction (2) is central to OCS hydrolysis, and our present studies show that reaction (2) is the main reaction path in the OCS hydrolysis. Further, several theoretical studies of the elementary processes and reaction mechanisms associated with reaction (2) are often contradictory. For example, studies of the gas-phase reaction of OCS with OH by high-level ab initio characterization of the potential surface have shown that the production of CO_2 and SH is the main pathway to the destruction of OCS by OH radicals [17, 18]. However, studies by Hu et al. [19] into the gas-phase reaction of OCS with OH radicals using DFT and the G3 method indicated that the production of CO and SOH was the main pathway. Furthermore, there is no mention in the literature [17–19] of the effect of bulk water solvent on the hydrolysis of OCS.

In the present work, to complete a comprehensive theoretical study of the hydrolysis mechanism of OCS and to gain a good understanding of the hydrolysis of OCS, we carried out a detailed theoretical investigation of the hydrolysis of OCS by reactions (1) and (2) in the presence of explicitly described OH^- and H_2O. In addition, the effect of the bulk water solvent on the reaction was also investigated using the conductor-like screening model (COSMO).

Computational methods

The structures of all stationary points (reactants, intermediates, transition states and products) involved in the reaction pathways of OCS hydrolysis were fully optimized at the level of the general gradient approximation (GAA) using the Becke–Lee–Yang–Parr correlation functional (BLYP) [20, 21]. The double-numeric quality basis set with polarization functions (DNP) was used; the size of the DNP basis set is comparable to Gaussian 6-31 G**, but the DNP basis set is more accurate than the Gaussian basis set of the same size. Moreover, this basis set is known to yield only a small basis set superposition error (BSSE) [22]. All stationary points were identified as minima (number of imaginary frequencies NIMAG=0) or transition states (NIMAG=1). The zero-point energy (ZPE) of each stationary point was also determined. The reaction pathways were examined by performing TS confirmation on most of the transition state structures to confirm that they lead to the desired reactants and products [23]. All calculations are performed with Dmol^3 using the Materials Studio 4.4 software package on an HP Proliant DL 380 G5 server system [24, 25].

The effect of the bulk solvent was investigated using the conductor-like screening model (COSMO) as implemented in Dmol^3 [26, 27]. This is a dielectric continuum solvation model in which the mutual polarization of the solute and solvent is represented by screening charges on the surface of the solute cavity. These charges are derived under the simplified boundary condition that the electrostatic potential vanishes for a conductor ($\varepsilon = 0$), and the charges are scaled to account for the finite dielectric permittivity of a real solvent. In this case, bulk water solvent is represented by a dielectric permittivity $\varepsilon = 78.54$.

Results and discussion

Evaluation of the computational accuracy

To evaluate the reliability of the chosen level of theory, we calculated the bond lengths and bond dissociation energies (BDE) for several species involved in reactions (1) and (2) using the GGA-BLYP functional. The relevant results are listed in Table 1, where the available experimental and calculated values are also presented for comparison. It is clear that the GGA-BLYP functional can provide satisfactory results, considering that our main goals in the present work are to examine the detailed hydrolysis mechanism and to calculate the relative energies of the species involved, not to calculate accurate bond energies.

Table 1 Theoretical and experimental bond lengths (Å) and bond dissociation energies (kJ mol^{-1})

Species	Calculated		Experimental
	GGA-BLYP	GGA-BLYP [a]	
OC–S	318.6	316.1	308.4 [b]
$R_{C–S}$	1.579	1.580	1.561 [c]
O–CS	689.6	687.8	664.9±0.85 [d]
$R_{C–O}$	1.176	1.172	1.156 [c]
C–S	701.0	699.6	712.2±0.85 [e]
O–C	1079.3	1071.1	1076.4±0.67 [b]
HS–H	384.1	–	381.4±0.50 [b]
HO–H	484.1	–	497.1±0.29 [b]

[a] From [28]
[b] From [29]
[c] From [30]
[d] From [31]
[e] From [32]

Reaction mechanism

There are two possible reaction pathways for the hydrolysis of OCS (O=C=S) in reaction (1). In the first, H_2O attacks across the C=O bond; in the other, H_2O attacks across the C=S bond. Research by Deng et al. [3] indicated that the addition of H_2O across the C=S bond is more favorable than its addition across the C=O bond. Thus, we will discuss the addition of an H_2O molecule across the C=S bond below. The optimized geometries for the reactants, intermediates, transition states, and products in reactions (1) and (2) are shown in Fig. 1, and the imaginary frequency of each transition state in the gas phase and bulk water solvent are summarized in Table 2. All bond distances are in Å and bond angles are in degrees, respectively.

OCS hydrolysis in the presence of H_2O

The reaction and activation energies for reaction (1) are listed in Table 3. The overall energetic profile is shown in Fig. 2. The nucleophilic attack of H_2O on the C atom of OCS leads to the formation of the precoordination complex IM1. IM1 is the reactant-like intermediate in which the geometries of two reactant molecules remain almost the same as for the corresponding free molecules. IM1 is 8.8 kJ mol^{-1} more stable than the original reactants OCS and H_2O. In the first step of the hydrolysis, the addition of H_2O to OCS is completed upon full hydrogen (H6) transfer from H_2O to S on OCS to form the thiocarbonic acid IM2 via a concerted transition state TS1 involving the cleavage of the O4–H6 bond and 1,3-hydrogen migration from O4 to S3. In TS1, the length of the O4–H6 bond that is broken is

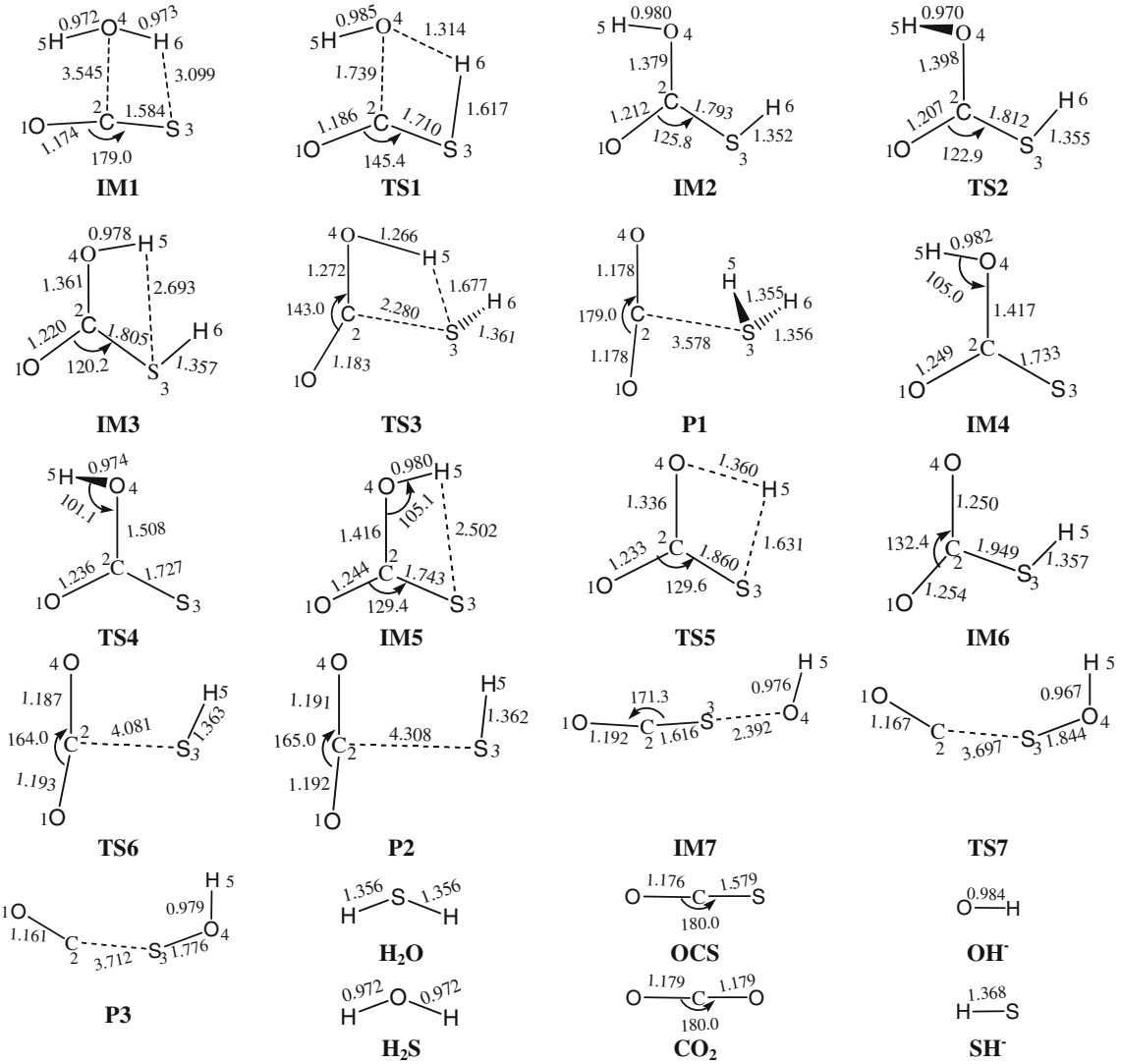

Fig. 1 Optimized geometries for the reactants, intermediates, transition states, and products involved in reactions (1) and (2) (distances in Å and angles in degrees)

Table 2 Imaginary frequency of each transition state in the gas phase and bulk water solvent

Transition states	Imaginary frequency (cm^{-1})	
	Gas phase	Bulk water solvent
TS1	−1383.9i	−1499.45i
TS2	−612.9i	−383.2i
TS3	−1521.0i	−1563.5i
TS4	−514.2i	−556.0i
TS5	−1409.1i	−1477.7i
TS6	−135.1i	−154.9i
TS7	−211.1i	−307.6i

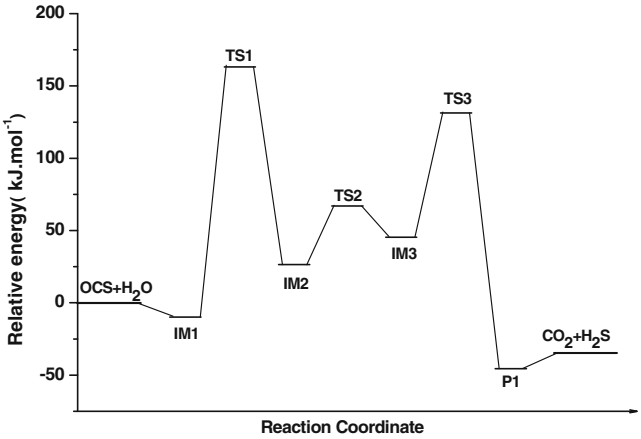

Fig. 2 Reaction energy profiles for the attack of H_2O on OCS

1.314 Å, and the angle O1–C2–S3 changes from 180.0° in OCS to 145.4°. The original linear OCS molecule is distorted. The H6–S3 and C2–O4 bonds that are formed have lengths of 1.617 and 1.739 Å, respectively. The C2–O4 bond shortens from 3.545 to 1.739 Å. The barrier height of TS1 relative to IM1 is 173.2 kJ mol^{-1}. Then, through a rotation along the O–H bond, IM2 is further converted to isomer IM3 via the transition state TS2. TS2 is 66.5 kJ mol^{-1} higher in energy than the reactants and 40.2 kJ mol^{-1} higher than the intermediate IM2. Finally, IM3 converts to P1, leading to the final products CO_2 and H_2S via a concerted transition state TS3 involving C2–S3 bond cleavage and 1,3-hydrogen (H5) migration from O4 to S3. TS3 is predicated to be 86.5 kJ mol^{-1} higher in energy than IM3.

According to the relative energies shown in Fig. 2, the activation barrier for TS1 is 173.2 kJ mol^{-1}, which is higher than those for TS2 and TS3 by 133.0 and 86.7 kJ mol^{-1}, respectively, indicating that the first step IM1→IM2 via TS1 is the rate-determining step (RDS) of reaction (1). Furthermore, Williams et al. [1] reported that at lower temperatures (303–333 K), the formation of thiocarbonic acid in the reaction of OCS with H_2O was experimentally found to be the RDS, suggesting that our calculated results are consistent with experimental results. The reverse reaction—the attack of H_2S on CO_2—appears to be similar to the attack of H_2O on OCS, and the corresponding activation barrier for the RDS is 177.0 kJ mol^{-1} (Fig. 2). Moreover, Fig. 2 also shows that the energy of (OCS + H_2O) is 26.7 kJ mol^{-1} higher than that of (CO_2 + H_2S), indicating that the reaction of OCS with H_2O is thermodynamically more favorable than the reverse reaction of H_2S with CO_2.

The mechanism for the hydrolysis of OCS with H_2O was found to be somewhat similar to that published earlier by Deng et al. [3]: the nucleophile H_2O approaches OCS, leading to the adduct IM1, and IM1 can then form the intermediate IM2 by hydrogen transfer from H_2O to S on OCS via a concerted transition state TS1, which is still the RDS. Then, IM2 evolves into another intermediate (IM3) and two transition states (TS2 and TS3), leading to the intermediate IM4, in which hydrogen transfer from O4 to S3 leads to the final product P1 via the transition state TS4. However, in our present studies, the calculated results show that the intermediate IM3 can directly form the final product P1 via a concerted transition state, and TS confirmation verifies that every transition state encountered in our studies is connected directly to the corresponding product and reactant. The activation barrier is 86.5 kJ mol^{-1}, which is much lower than the 126.1 kJ mol^{-1} obtained by Deng et al. Therefore, we can confirm that the mechanism of reaction (1) in our studies has some improvements, and differs to some degree from that obtained in the studies of Deng et al.

OCS hydrolysis in the presence of OH^-

The reaction mechanism of OCS with OH^- is different from that with H_2O; it is somewhat analogous to that of OCS with

Table 3 Activation and reaction energies for reaction (1) in the gas phase and bulk water solvent

Elementary step	Gas phase		Bulk water solvent	
	E_a (kJ mol^{-1})	ΔE (kJ mol^{-1})	E_a (kJ mol^{-1})	ΔE (kJ mol^{-1})
IM1→IM2	173.2	17.6	178.8	38.7
IM2→IM3	40.2	19.7	29.3	4.6
IM3→P1	86.5	−90.5	110.7	−63.5

the OH radical proposed by Danielache et al. [18], involving common isomerization and a hydrogen transfer step. However, the reaction process and intermediates are mostly different; in particular, the hydrogen thiocarbonate ($HSCO_2^-$) intermediate is not obtained, which is a key intermediate in experimental studies of OCS adsorbed on an alumina surface at basic hydroxyl groups [9, 10] and magnesium oxide with surface hydroxyls [33]. The reaction and activation energies related to reaction (2) are listed in Table 4.

Figure 3 shows an energy profile for the carbon-bonded adducts, as OCS is a polar molecule with high positive charge on the C atom, while there is a strong negative charge on the O atom in OH^-. Thus, the addition of OH^- to the carbon gives the carbon-bond adduct IM4. The formation of IM4 is highly exothermic (by 268.5 kJ mol^{-1}) relative to the reactants OCS and OH^-. A transition state for the formation of IM4 from the reactants could not be located; all attempts to locate this species invariably converged to the structure of IM4. Our calculations therefore confirm that the attack of OH^- on the C atom of OCS can directly produce the carbon-bonded adduct IM4.

Starting from IM4, an internal rotation of the OH group in IM4 results in the rotational isomer IM5 via the transition state TS4 with an activation energy of 32.3 kJ mol^{-1}. IM5 is planar with the OH oriented toward sulfur, which is 13.5 kJ mol^{-1} lower in energy than IM4. TS4 is the only nonplanar structure; in this, the OH projects above the plane with a dihedral angle (H5–O4–C2–S3) of −97.9°, and the angle between OH and the C atom (H5–O4–C2) is 101.0°. Internal transfer of the hydrogen atom from the OH in IM5 to sulfur via a planar four-membered ring transition state TS5 where the hydrogen atom is shared between the oxygen and sulfur atoms leads to hydrogen thiocarbonate IM6 ($HSCO_2^-$), which is in agreement with previous experimental studies [9, 10]. In TS5, the O4–H5 and C2–S3 bonds elongate from 0.980 to 1.360 Å and from 1.743 to 1.860 Å, respectively. The C2–O4 and S3–H5 distances shorten from 1.416 to 1.336 Å and from 2.502 to 1.631 Å, respectively. This step has an activation barrier of 56.6 kJ mol^{-1}, and IM6 is 35.1 kJ mol^{-1} more stable than IM5. Finally, a transition state, TS6, with C–S bond cleavage for the decomposition of IM6 to P2 was located. This step was found to be endothermic by 77.9 kJ mol^{-1}, with an activation energy of 73.1 kJ mol^{-1}. As shown in Fig. 3,

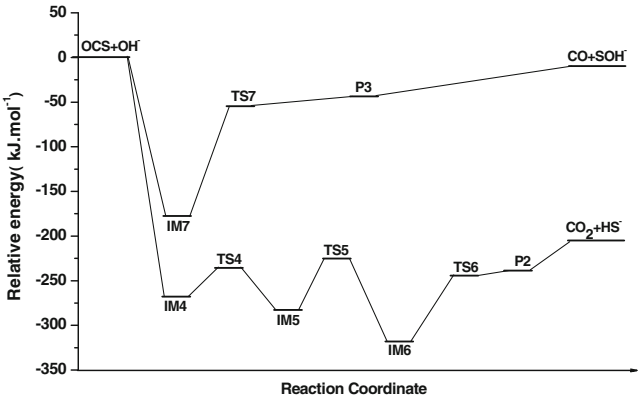

Fig. 3 Reaction energy profiles for the attack of OH^- on OCS

the activation energy for TS6 is 73.1 kJ mol^{-1}, which is higher than TS4 and TS5 by 40.8 and 16.5 kJ mol^{-1}, respectively, indicating that the IM6→P2 step via the transition state TS6 with C–S bond cleavage is the RDS for reaction (2). This is in agreement with the reported experimental results. For example, at a higher temperature (523 K), the reaction follows Langmuir–Hinshelwood kinetics, where the surface hydrolysis of hydrogen thiocarbonate with C–S bond cleavage is the RDS [1, 16].

In addition, Fig. 3 also shows an energy profile for the sulfur-bonded adduct. The addition of OH^- to the sulfur of OCS directly gives sulfur-bond adduct IM7, and P3 is formed from IM7 via the transition TS7. IM7 is highly exothermic (by 176.9 kJ mol^{-1}) relative to the reactants OCS and OH^-. This reaction has an activation energy of 122.4 kJ mol^{-1}. Given the wide-scale rearrangement of atoms in this reaction, the formation of the sulfur-bonded adducts CO and SOH^- is endothermic and not stable with respect to IM7. Thus, any collision sulfur-bond complex of OCS and OH^- would be likely to decompose spontaneously back to IM7. Experiments by Leu and Smith [34] detected that SOH was only a minor product of the reaction of OCS and OH. The results calculated above show that CO_2 and SH^- are the main products for reaction (2). Moreover, the experiment by Leu and Smith indicated that SH was formed as a major product of the reaction of OCS with OH at 517 K.

Based on the above analyses of the hydrolysis mechanisms of OCS, we can see that the RDSs of

Table 4 Activation and reaction energies of reaction (2) in the gas phase and bulk water solvent

Elementary step	Gas phase		Bulk water solvent	
	E_a (kJ mol^{-1})	ΔE (kJ mol^{-1})	E_a (kJ mol^{-1})	ΔE (kJ mol^{-1})
IM4→IM5	32.3	−13.5	32.8	−6.3
IM5→IM6	56.6	−35.1	73.6	−29.6
IM6→P2	73.1	77.9	37.8	64.8

Table 5 Effect of temperature on the Gibbs free energy changes ΔG and equilibrium constants K for reactions (1) and (2)

Reaction		Temperature (K)				
		298.15	300	400	500	600
1	ΔG (kJ mol^{-1})	−41.0	−41.0	−38.2	−35.1	−31.9
	K	1.53×10^{7}	1.35×10^{7}	9.68×10^{4}	4.68×10^{3}	5.98×10^{2}
2	ΔG (kJ mol^{-1})	−198.0	−198.0	−198.0	−198.4	−199.3
	K	4.91×10^{34}	3.00×10^{34}	7.12×10^{25}	5.39×10^{20}	2.26×10^{17}

reactions (1) and (2) are the elementary steps via TS1 and TS6, respectively. The corresponding activation energies for these steps are 173.2 and 73.1 kJ mol^{-1}, respectively. The activation energy of TS1 is much higher than that of TS6, suggesting that reaction (2) is more favorable in terms of dynamics than reaction (1). Therefore, it can be concluded that reaction (2) is the main reaction path for the hydrolysis of OCS.

Effect of temperature on the thermodynamic quantities of the reactions

The total Gibbs free energy changes and equilibrium constants for reactions (1) and (2) calculated at different temperatures are listed in Table 5. Our study covers the temperature range 298.15–600 K.

From Table 5, it can be seen that reaction (2) is always the easiest at any temperature as it has the smallest ΔG at different temperatures. It always makes the greatest contribution to the hydrolysis of OCS, and reaction (1) always makes the next largest contribution; this sequence does not change with increasing temperature. In addition, for reactions (1) and (2), the calculated equilibrium constants decrease as the temperature increases, suggesting that OCS hydrolysis should proceed more favorably at low temperatures. Taking the reported experimental results [1, 16] into account, we can conclude that at lower temperatures, reactions (1) and (2) are responsible for the hydrolysis of OCS (as supported by thermodynamic quantities), and that reaction (2) is the main reaction. At higher temperatures, reaction (2) mainly contributes to the hydrolysis of OCS.

Using the calculated results for the above thermodynamic quantities, the specific mechanism of hydrolysis for OCS was elucidated in the temperature range 298.15–600 K, and this hydrolysis mechanism was found to be very close to that found experimentally. However, we cannot only consider the effect of temperature on the thermodynamic quantities associated with the hydrolysis of OCS; we must also study the effect of temperature on the kinetic quantities associated with this hydrolysis reaction.

The rate constants for reactions (1) and (2)

As mentioned above, reaction (2) may be the main pathway for the hydrolysis of OCS. To understand the hydrolysis of OCS at different temperatures from a kinetics perspective, the rate constants for the RDSs of reactions (1) and (2) were calculated in the temperature range 298.15–600 K. The rate constants were obtained using Eyring's transition state theory (TST) [35, 36], and the relevant data are listed in Table 6.

According to the data in Table 6, the rate constant k increases rapidly with the temperature, but the rate of increase drops at higher temperatures. The rate constant of reaction (2) is much larger than that of reaction (1) at the same temperature, and this does not change if the temperature is modified, which implies that reaction (2) is faster than reaction (1).

The results calculated above show that the hydrolysis of OCS in the presence of OH^- is the main reaction pathway from thermodynamic and kinetic standpoints, and is responsible for the hydrolysis of OCS. OH^- plays a critical role in the hydrolysis of OCS, as confirmed by the experimental observation that OH^- triggers and encourages the hydrolysis of OCS [16, 37]. These calculated results provide us with a microscopic illustration of and theoretical guidance for the hydrolysis of OCS.

Table 6 The calculated rate constants k (cm^3 mol^{-1} K^{-1}) for the reactions (1) and (2)

Reaction	Temperature (K)				
	298.15	300	400	500	600
1	3.66×10^{-19}	5.50×10^{-19}	7.06×10^{-12}	1.32×10^{-7}	9.49×10^{-5}
2	3.72×10^{3}	4.40×10^{3}	3.78×10^{6}	2.20×10^{8}	3.28×10^{9}

Analysis of the effect of temperature on the thermodynamic and kinetic results

Based on the above thermodynamic and kinetic results, we can conclude that the percentage conversion of the reactants is the major consideration for the thermodynamics of the hydrolysis reaction; a lower temperature favors the hydrolysis of OCS. The reaction velocity of the reactants is the major consideration for the kinetics of the reaction; a higher temperature can accelerate the hydrolysis of OCS. Generally, there is not necessarily a relationship between the reaction velocity and the percentage conversion of the reactant. However, we can be sure that the hydrolysis of OCS is influenced by the thermodynamics and kinetics of the reaction. Therefore, for the hydrolysis of OCS, the reaction temperature should lie in a reasonable range that will lead to not only a high conversion rate but also a fast reaction.

Effect of the solvent

The literature [38–41] has shown that chemical characteristics and reactions can be influenced by the nature of the solvent used. In order to study the effect of the solvent, OCS hydrolysis via reactions (1) and (2) was examined in bulk water solvent using the COSMO model (dielectric constant ε=78.54), employing the geometries optimized in the gas phase. The reaction and activation energies after correcting for bulk solvent effects are listed in Tables 3 and 4.

As listed in the tables, for reaction (1), when the activation energy values of the RDS in the gas phase are compared with those obtained after COSMO treatment, it becomes apparent that the bulk solvent does not modify the RDS, and it barely modifies its activation energy. For example, the activation energy is 173.2 kJ mol^{-1} in the gas phase but 178.8 kJ mol^{-1} in bulk water solvent. This similarity in values probably arises because most of the solvent effect is already taken into account when just one water molecule is considered. Our calculated results are in agreement with the results of Deng et al. [3], who found that the bulk water solvent does not change the calculated energy barriers of the OCS hydrolysis reaction with five waters significantly when using the PCM solvation model. However, for reaction (2), the effect of the bulk solvent can change the RDS from the elementary step IM6→P2 in the gas phase to the elementary step IM5→IM6 in bulk water solvent. Again, however, the corresponding activation energies barely change: 73.1 kJ mol^{-1} for IM6→P2 in the gas phase to 73.6 kJ mol^{-1} for IM5→IM6 in bulk water solvent. The calculated results for reaction (2) suggest that the solvent can influence the RDS, but it still barely modifies the activation energy of the RDS. The above results on the effect of the solvent on the hydrolysis of OCS show that the effect of the bulk water solvent on the hydrolysis of OCS can be taken into account by simply making OCS react with a single water molecule or a hydroxyl ion.

Conclusions

In this study, a comprehensive mechanistic investigation of the hydrolysis of OCS, including the reactions of OCS with H_2O and OH^-, was undertaken by performing DFT calculations in both the gas phase and bulk water solvent. The effect of the bulk water solvent was taken into account using the COSMO model. The calculated results show that the reaction of OCS with H_2O proceeds via an addition–elimination mechanism controlled by the formation of hydrogen thiocarbonic acid, as observed in the reported experiment. For the reaction of OCS with OH^-, the calculated results suggest that carbon-bonded adduct reaction is the main pathway for the destruction of OCS by OH^-. The reaction of OCS with OH^- is mainly responsible for the hydrolysis of OCS. When the activation energies for the RDSs of reactions (1) and (2) in the gas phase were compared with those obtained after COSMO treatment, we found that the bulk solvent has a relatively small effect, probably because most of the solvent effect is already taken into account when we consider a water molecule or a hydroxyl ion, thus indicating that the hydrolysis of OCS can be considered to be the reaction of OCS with just a single water molecule or a hydroxyl ion.

Based on our results, which indicate that the reaction of OCS with OH^- is the main contributor to the hydrolysis of OCS, we believe that in the hydrolysis of OCS under realistic reaction conditions on metal oxide surfaces such as Al_2O_3, the intrinsic properties of the Al_2O_3 and the pretreatment conditions will affect the hydroxyl coverage. Furthermore, varying the reaction conditions will change the partial pressure of water, thus affecting the hydroxyl coverage of the Al_2O_3 surface. As a result, higher coverage of hydroxyls on the Al_2O_3 surface will promote the hydrolysis of OCS, leading to the elimination and removal of environmental sulfur-containing pollutants like carbonyl sulfide as CO_2.

Acknowledgments This work was supported financially by the National Basic Research Program of China (no. 2005CB221203), the National Natural Science Foundation of China (no. 20976115 and 20776093) and the Younger Foundation of Shanxi Province (no. 2009021015).

References

1. Williams BP, Young NC, West J, Rhodes C, Hutchings GJ (1999) Catal Today 49:99–104
2. Deng C, Wu XP, Sun XM, Ren Y, Sheng YH (2009) J Comput Chem 30:285–294

3. Deng C, Li QG, Ren Y, Wong NB, Chu SY, Zhu HJ (2008) J Comput Chem 29:466–480
4. Fiedorow R, Leaute R, Dalla LIG (1984) J Catal 85:339–348
5. Liang MS, Li CH, Guo HX, Xie KC (2002) Chin J Catal 23:357–362
6. Nnmba S, Shiba T (1968) Kogyo Kagaku Zasshi 71:93–96
7. Zhang YQ, Xiao ZB, Ma JX (2004) Appl Catal B Environ 48:57–63
8. Zhang QL, Guo HX (1988) Chin J Catal 9:14–24
9. He H, Liu JF, Mu YJ, Yu YB, Chen MX (2005) Environ Sci Technol 39:9637–9642
10. Liu JF, Yu YB, Mu YJ, He H (2006) J Phys Chem B 110:3225–3230
11. Wu HB, Wang X, Cheng JM (2004) Sci China Ser B 32:127–132
12. Wu HB, Wang X, Cheng JM, Yu HK, Xue HX, Pan XX, Hou HQ (2004) Chin Sci Bull 49:739–743
13. Dykstra C, Frenking G, Kim K, Scuseria G (2005) Theory and applications of computational chemistry. Elsevier, Amsterdam
14. Yang T, Wen XD, Huo CF, Li YW, Wang JG, Jiao HJ (2009) J Mol Catal A Chem 30:129–136
15. Aboulayt A, Maugé F, Hoggan PE, Lavalley JC (1996) Catal Lett 39:213–218
16. Hoggan PE, Aboulayt A, Pieplu A, Nortier P, Lavalley JC (1994) J Catal 149:300–306
17. Wilson C, Hirst DM (1995) J Chem Soc Faraday Trans 91:793–798
18. Danielache SO, Johnson MS, Nanbu S, Grage MML, McLinden C, Yoshida N (2008) Chem Phys Lett 450:214–220
19. Hu WH, Shen W, Xu JH (2006) J Sichuan Normal Univ (China) 29:336–339
20. Becke AD (1988) J Chem Phys 88:2547–2553
21. Lee C, Yang W, Parr RG (1988) Phys Rev B 37:785–789
22. Sauer J (1992) In: Catlow CRA (ed) Modeling of structure and reactivity in zeolites. Academic, London, pp 206–207
23. Zhang RG, Huang W, Wang BJ (2007) Chin J Catal 28:641–645
24. Delley B (1990) J Chem Phys 92:508–517
25. Delley B (2000) J Chem Phys 113:7756–7764
26. Klamt A, Schrmann G (1993) J Chem Soc Perkin Trans 2:799–805
27. Klamt A, Jonas V, Bürger T, Lohrenz JCW (1998) J Phys Chem A 102:5074–5085
28. Gao LG, Song XL (2007) J Mol Struc (THEOCHEM) 820:12–17
29. Luo YR (2005) Handbook of chemical bond dissociation energies. Science, Beijing
30. Lahaye JG, Vandenhaute R, Fayt A (1987) J Mol Spectrosc 123:48–83
31. Pedley JB, Naylor RD, Kirby SP (1986) Thermochemical data of organic compounds. Chapman and Hall, London
32. Prinslow DA, Armentrout PB (1991) J Chem Phys 94:3563–3567
33. Liu YC, He H, Xu WQ, Yu YB (2007) J Phys Chem A 111:4333–4339
34. Leu MT, Smith RH (1981) J Phys Chem 85:2570–2575
35. Fu XC, Shen WX, Yao TY (1990) Physical chemistry, 4th edn. Higher Education, Beijing
36. Wang BJ, Wei XY, Xie KC (2004) Chin J Chem Eng 55:569–574
37. Liu JF, Liu YC, Xue L, Yu YB, He H (2007) Acta Phys Chim Sin 23:997–1002
38. de Lima EF, de Carneiro MJW, Fenollar-Ferrer C, Miertus S, Zinoviev S, Om Tapanes NC, Aranda DAG (2010) Fuel 89:685–690
39. Tomasi J, Mennucci B, Cammi R (2005) Chem Rev 105:2999–3094
40. Sanna N, Chillemi G, Grandi A, Castelli S, Desideri A, Barone V (2005) J Am Chem Soc 127:15429–15436
41. Sebek J, Kejik Z, Bour P (2006) J Phys Chem A 110:4702–4711